Desalination and Water Treatment
www.deswater.com

doi: 10.5004/dwt.2023.29323

286 (2023) 160–172
February

Degradation of bisphenol A in Fe-doped layered double hydroxide activated persulfate systems by enhancing with hydroxylamine hydrochloride

Shuwang Zhang[a], Luping Zhang[a], Jialing Zhao[a], Wenying Yuan[a], Xing Fang[a], Qianqian Yu[b], Jing Cheng[a,*], Xinhong Qiu[a,c,*]

[a]*School of Chemistry and Environmental Engineering, Wuhan Institute of Technology, Wuhan, China, Tel.:/Fax: (86) 27 8719 5680; emails: Jeannie1204@126.com (J. Cheng), qxinhong@gmail.com (X. Qiu), 443432659@qq.com (S. Zhang), 443432659@qq.com (L. Zhang), 2269341164@qq.com (J. Zhao), 3013408422@qq.com (W. Yuan), 1052681371@qq.com (X. Fang)*
[b]*School of Earth Science, China University of Geosciences, Wuhan 430074, China, email: qianqianyu09@gmail.com*
[c]*Hubei Engineering Technology Research Center for Chemical Industry Pollution Control*

Received 18 November 2022; Accepted 24 January 2023

ABSTRACT

In this study, the degradation of bisphenol A (BPA) was enhanced by adding the reducing agent hydroxylamine hydrochloride (HAHC) into the layered double hydroxides (LDH)/peroxymonosulfate (PMS) system to promote the conversion of ferric iron (Fe(III)) to Fe(II). The results showed that the degradation efficiency exceeded 90% within 120 min after the addition of HAHC. The effects of initial BPA, PMS concentration, and LDH dosage on BPA degradation efficiency were also evaluated in the HAHC/LDH/PMS system. In addition, the catalyst showed high catalytic activity over a wide pH range (2~10) within the experiment. Radical scavenging tests confirmed that the main reactive oxygen species were sulfate radical ($SO_4^{\bullet-}$), hydroxyl radical ($^{\bullet}OH$) and superoxide radical ($O_2^{\bullet-}$) in the HAHC/LDH/PMS process. The reaction mechanism was also inferred by using various analytical techniques, including X-ray photoelectron spectroscopy, X-ray diffraction, electron paramagnetic resonance, scanning electron microscopy, transmission electron microscopy, liquid chromatography–mass spectrometry. This work provides a new strategy for the degradation of organic pollutants by the addition of HAHC to promote the activation of PMS by catalysts.

Keywords: Layered double hydroxides; Persulfate; Bisphenol A; Hydroxylamine hydrochloride; Reactive oxygen species

1. Introduction

Due to the inability of traditional treatment technologies to completely remove toxic contaminants from water, coupled with the growing demand for high-quality clean water, people are focusing on developing more efficient water treatment technologies [1]. Recently, advanced oxidation technology, which can efficiently degrade organic pollutants, has received more and more attention, and advanced oxidation technology based on sulfate radicals ($SO_4^{\bullet-}$) has been increasingly applied to various water remediation (e.g., groundwater, drinking water and wastewater) [2,3]. It replaces conventional hydrogen peroxide (H_2O_2) with peroxymonosulfate (PMS), which decomposes HSO_5^- in the presence of a catalyst to generate sulfate radicals ($SO_4^{\bullet-}$) [4]. Compared with the $^{\bullet}OH$-based degradation process, this $SO_4^{\bullet-}$-driven degradation process has many advantages. These include the fact that $SO_4^{\bullet-}$ has standard redox potential (2.5–3.1 V) close to or even higher than that of $^{\bullet}OH$ (2.8 V), and has a longer half-life (4 s) than that of the hydroxyl radical (below 1 μs) [5–8]. Moreover, $SO_4^{\bullet-}$ can degrade some difficult organic pollutants more effectively because of its higher selectivity than $^{\bullet}OH$ [9,10]. Therefore, the activation of PMS to generate

* Corresponding author.

$SO_4^{\bullet-}$ to degrade organic pollutants has been extensively studied [11–15].

With the presence of light, heat and transition metal ions, persulfate ion is activated to sulfate radicals owing to the breakage of the peroxy group (O–O) [16–19]. The common activation methods are thermal activation, alkali activation, UV activation, transition metal ion and metal oxide activation, carbonaceous material activation. Among the various activation methods, transition metals are of great interest for their convenience, efficiency and low cost, among which Ag^+, Co^{2+} and Fe^{2+} have shown better performance in PMS activation [20,21]. However, the following problems are inevitable in the homogeneous system: Firstly, the presence of a large number of metal ions in the wastewater, which generates secondary pollution [22]. Then, the pH of the solution has a strong influence on the composition and content of metal ions [23]. Moreover, some organic substances may complex with metal ions leading to a lower activation efficiency [24]. In practical application, Fe(II) is usually chosen as activator of PMS to generate $SO_4^{\bullet-}$ for the advantages of environment-friendly, cost-effective and high activity, while the heterogeneous system overcomes the above problems to a certain extent [25,26].

In heterogeneous systems, the activation performance of catalysts usually changes with the surface properties of materials. Recently, many studies have been carried out to synthesize heterogeneous materials for PMS activation, and high efficient degradation effect has been achieved [27,28]. In addition to synthetic materials, natural minerals can also be used for heterogeneous activation, such as magnetite and siderite [29,30]. 85% of dichlorophenol was degraded by Fe_2O_3-montmorillonite synthesized by coprecipitation and calcination, exhibiting that the composite materials had high catalytic activity for PMS [31]. Hou synthesized high crystallinity MnFe-LDH to active PMS to degrade Acid Orange 7 (AO7), the system indicated 97.56% contaminant had been mineralized with a lower dosage (0.20 g/L). X-ray photoelectron spectroscopy (XPS) of the catalyst which before and after reacted illustrated synergistic effect was between Mn and Fe [32]. Liu et al. [33] reported heterogeneous Fe-based layered double hydroxide as PMS activators to completely degrade 500 mg/kg isoproturon in soil within 10 h. The catalyst can not only be used in a wide pH range (3~11), but also can accommodate a variety of inorganic ions and humic acids.

Using heterogeneous catalysts effectively avoids the accumulation of iron oxide sludge and extends the range of pH. However, the issue of the slow transformation from Fe(III) to Fe(II) still remains in heterogeneous systems [34]. Therefore, previous studies have shown that the addition of some reducing agents promotes the conversion of Fe(III) to Fe(II) to improve the removal efficiency of organic pollutants. Wu et al. [35] added different reducing agents (hydroxylamine (HA), sodium thiosulfate, ascorbic acid, sodium ascorbate and sodium sulfite) into PS/HA system to improve the degradation efficiency of trichloroethylene (TCE) by accelerating the transformation from Fe(III) to Fe(II). Using benzoic acid (BA) as the target pollutant, Zou et al. investigated that HA could promote the Fe(II) regeneration in Fe(II)/PMS process to accelerate the degradation of BA [36]. And these results indicated hydroxylamine (HA) was a strong reducing agent for reducing Fe(III) to Fe(II). Moreover, hydroxylamine hydrochloride (HAHC) was used for the determination of Fe(II) concentration by the spectrophotometric method using 1,10-phenanthroline [37]. Miao et al. [38] have inferred that the addition of HAHC enhanced the degradation of TCE in the Fe(II)/Fe(III) catalyzed sodium percarbonate (SPC) system. Interestingly, layered double hydroxides (LDHs) are widely used as catalysts due to their excellent selectivity, high activity, high dispersion and high reusability, thus enabling multiphase reactions [39,40]. Fe(II)-Al-LDH can be used as an environmentally friendly heterogeneous catalyst [41], while not avoiding its easy oxidation property.

Herein, in this paper, using synthesized Fe-doped MgAl hydrotalcite to investigate the effect of hydroxylamine hydrochloride on bisphenol A (BPA) degradation efficiency in the LDH/PMS process with the addition of HAHC. The specific objectives were to (1) successfully synthesize hydrotalcite with various contents of Fe, and compare the characterization of the materials before and after the reaction; (2) study the effect of different conditions on the degradation of BPA; (3) identify major reactive oxygen species; (4) test the reusability and stability of MgAlFe-LDH catalyst.

2. Experiment set-up

2.1. Chemical

Ferric nitrate ($Fe(NO_3)_3{\cdot}9H_2O$), magnesium nitrate ($Mg(NO_3)_2{\cdot}6H_2O$), aluminum nitrate ($Al(NO_3)_3{\cdot}9H_2O$), urea (CON_2H_4), formamide sodium hydroxide (NaOH), hydrochloric acid (HCl), bisphenol A (BPA), ethyl alcohol (C_2H_6O), T-butanol ($C_4H_{10}O$), and *p*-benzoquinone ($C_6H_4O_2$) used in this experiment were analytical grade reagents and purchased from Sinopharm Chemical Reagent Co., Ltd., (China). Potassium peroxymonosulfate ($KHSO_5{\cdot}0.5KHSO_4{\cdot}0.5K_2SO_4$, PMS) were of analytical grade and supplied by Aladdin Chemistry Co., Ltd., (Shanghai, China). All the chemical solutions were prepared with ultrapure water (18.25 MΩ·cm) by a water purified system (UPT-II-10T, ULUPURE, China).

2.2. Synthesis of LDH

MgAlFe-CO_3LDHs were synthesized by the urea method. All the samples kept the molar ratio of divalent to trivalent metal at 2:1 to obtain higher stability crystalline LDH construction. And the corresponding *x*%Fe-LDHs samples, where x = 0.07, 0.12, 0.16, 0.23 and 0.7, were denoted as 0.7%Fe-LDH. For instance, to prepare 0.3%Fe-LDH, 4.29 g of $Mg(NO_3)_2{\cdot}6H_2O$, 3.09 g of $Al(NO_3)_3{\cdot}9H_2O$, 0.1014 g of $Fe(NO_3)_3{\cdot}9H_2O$ and 4.90 g of urea were dissolved in 50 mL water. Then, the mixed solution was transferred into 100 mL Teflon vessel and crystallized in a 100°C oven for 36 h. The precipitate was collected by centrifugation at 9,000 rpm for 5 min and washed three times with deionized water. The sample was desiccated at 50°C in an oven. Other LDHs were prepared in the similar way by varying x according to the designed value.

2.3. LDH-activated PMS oxidation of BPA

The experiment was carried out in a glass beaker with a capacity of 250 mL and placed on a magnetic stirrer

under 25°C. A certain amount of LDH that had reduced by hydroxylamine hydrochloride (HAHC) and potassium peroxymonosulfate (PMS) were added into 100 mL BPA solution with the concentration of 20 mg/L and pH 7 adjusted in advance, in which the initial concentrations of hydroxylamine hydrochloride, LDH and peroxymonosulfate were 1 g/L and 10 mmol/L, respectively.

Initial experiments were conducted to observe the feasibility of activating PMS by LDH with different iron content. To determine the effect of Fe-LDH dosages on BPA degradation, Fe dose varied from 0.25 to 2.0 g/L. To identify the effect of PMS concentration on BPA degradation, the concentration of PMS varied from 0.1 to 1.5 g/L. Subsequently, the effect of initial concentration and pH (2, 5, 7, 10, and 12) on BPA degradation efficiency was also discussed.

1 mL solution was taken out each time at 5, 15, 30, 60, 90, and 120 min and filtered through 0.45 μm organic membrane, used to determine the residual concentration of bisphenol A by high-performance liquid chromatography (HPLC) (P3100, Elite, Dalian). The detection wavelength was set at 278 nm. The separation of BPA in the mixture was carried out by using a SinoChrom C18-ODS-BP column (5 μm, 4.6 mm × 250 mm) at room temperature. The mobile phase consisted of a mixture of methanol and water (70:30 v/v) with a total operating time of 15 min at a flow rate of 1.0 mL/min. The solid was collected by a sand core filter with 0.45 μm organic membrane, used for recycling reaction and characterization. Each experiment of BPA degradation was repeated two to three times to ensure its repeatability.

2.4. Characterization

The crystalline phase of MgAlFe-CO_3LDHs was determined using a D8 Advance X-ray diffractometer (XRD) (Bruker, Germany) with Cu/Kα radiation (30 kV, 20 mA) at 0.02° step size. The surface morphologies of different samples were obtained by using a JSM-5510LV scanning electron microscopy (SEM) (JEOL, Japan) at an accelerating voltage of 10 kV. The size and morphology of the LDHs were observed using a JEM-2100 transmission electron microscopy (TEM) (JEM-2100, JEOL, Tokyo, Japan). In addition, the variations of the electronic binding energy of iron and oxygen elements were analyzed using an X-ray photoelectron spectrometer (XPS) (Escalab 250XI, ThermoFisher, USA). An electron paramagnetic resonance (EPR) spectrometer (Bruker EMXPLUS, Germany) with a spin-trapping agent DMPO was used to identify the free radicals in solution. BPA degradation products were identified by ultrahigh performance liquid chromatograph (Agilent 1290 UPLC) coupled to a Agilent QTOF 6550 mass spectrometry with C-18 column (1.7 um, 2.1 mm × 50 mm). The mass spectrometer was operated in the positive (+) electrospray ionization mode (ESI) with m/z scans ranging from 50 to 1,000.

3. Results and discussion

3.1. Characterization

Fig. 1a shows that all primary samples with various Fe contents formed a typical layer structure of LDHs. XRD pattern of pristine sample formed a typical layer structure with well-defined diffraction peaks (003, 006, 009, 015, 110, 113) occurring at 2θ = 11.9°, 24.0°, 35.7°, 40.5°, 62.4° and 63.7°, respectively. The patterns indicated that a series of sharp and intense symmetrical diffraction peaks at low 2θ values and clear reflections at high 2θ values, suggesting the raw materials have regular structure and high crystallinity. Interestingly, because of the low content of Fe(III) in LDH (rang from 0.07% to 0.7%), its structure was closer to binary MgAl-LDH [42].

The Fourier-transform infrared (FTIR) spectra of primary MgAlFe-LDH are shown in Fig. 1b. Bands in the range of 3,300 to 3,500 cm^{-1} were assigned to the stretching vibration of interlayer –OH group. The band at near 1,629 cm^{-1} was identified to the bending vibration of interlayer adsorbed water molecules. The strong characteristic absorption band at 1,354 cm^{-1} was ascribed to the stretching vibration of C–O in CO_3^{2-}. The absorption band at 500 ~ 800 cm^{-1} was deemed to the stretching vibration of the metal-oxygen-metal bond, corresponding to the vibration of Al–O, Mg–O and Fe–O [43].

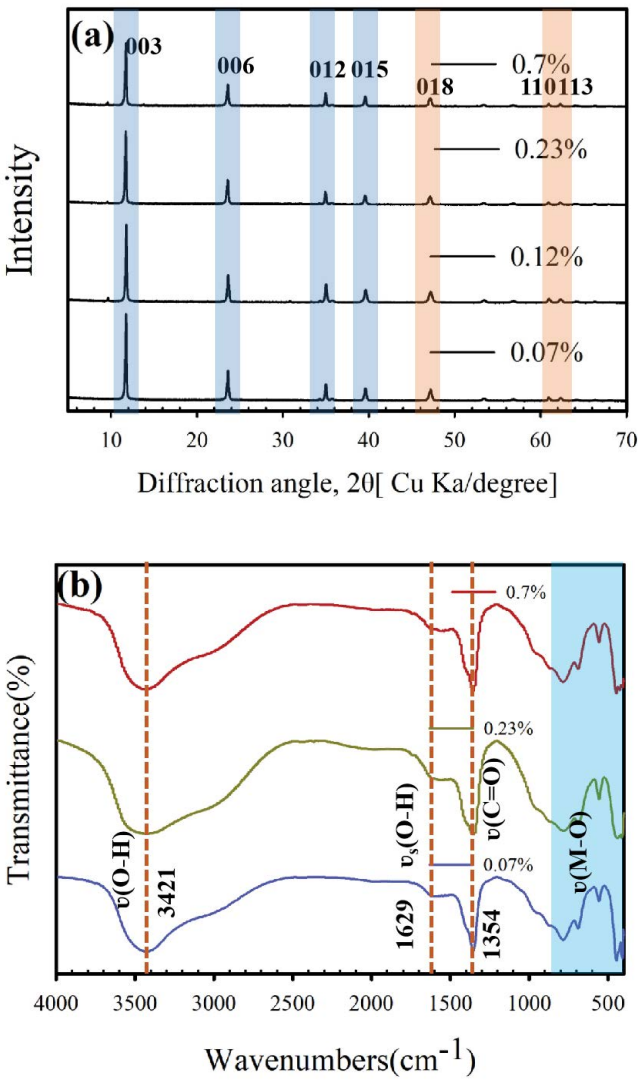

Fig. 1. (a) XRD spectra of primary MgAlFe-LDH and (b) FTIR spectra of primary MgAlFe-LDH.

The SEM images of primary MgAlFe-LDH are presented in Fig. 2. It can be found that materials exhibited a hexagonal sheet-like morphology. Compared with Mg_3-Fe_1-CO_3LDH, bigger size and more "collapses" don't show up as the ratio of Fe/Al increased. Because of the low content of Fe(III) in LDH (rang from 0.07% to 0.7%), its structure and morphology were closer to binary MgAl-LDH [44].

From the TEM image (Fig. 2), the primary material displayed a clear hexagonal lamellar overlay with the black spots on the surface representing the metals of Mg, Al, and Fe.

Fig. 3 shows XPS spectra of primary MgAlFe-LDH. The synthesized material contained Mg, Al, O, C and a small amount of Fe corresponding to the characteristic peaks of Mg 1s, Al 2p, O 1s, C 1s and Fe 2p in the XPS full spectrum. Due to the low proportion of Fe doping in the material, the 2p electronic signal of Fe in XPS data was relatively weak and the peak intensity was low. As shown in Fig. 3b, the two peaks of electron binding energy at 712 and 728 eV corresponded to the two main peaks of Fe $2p_{3/2}$ and Fe $2p_{1/2}$, respectively. The peaks with binding energies appearing at 712.4 and 709.7 eV were attributed to the presence of Fe^{3+} ions and Fe^{2+}, respectively. The presence of partially divalent iron was caused by a vacuum-induced reduction [45].

3.2. BPA degradation performance in HAHC/MgAl-Fe(III)/PMS system

3.2.1. Degradation efficiency of BPA in HAHC/MgAl-Fe(III)/PMS system

Fig. 4 shows the degradation of BPA in the HAHC/MgAl-Fe(III)/PMS Process. It had demonstrated that MgAl-LDH and Fe-doped MgAl-LDH had no adsorption effect on BPA, which the removal efficiency of BPA were 3.5% and 5.0%, respectively. As can be seen, a few degradation of BPA was observed in presence of PMS alone, while BPA removal rate increased obviously as PMS activated by Fe^{2+} or MgAl/MgAl-0.12%Fe(III). Such result could be interpreted with the low adsorption capacity of MgAl, the low Fe(II) concentration, a rapid accumulation of Fe(III), the slow transformation from Fe(III) to Fe(II) and the formation of Fe(III) precipitates as iron oxide or hydroxide at pH > 4 [46]. Furthermore, the degradation efficiency of BPA in the MgAl-*x*%Fe(III)/PMS system without hydroxylamine hydrochloride was only 50.6%. Surprisingly, more than 80% of BPA was degraded in 30 min in the MgAl-Fe(III)/PMS process with the addition of HAHC, indicating the enhancement effect of HAHC. Compared to that of undoped-Fe(III) (MgAl/PMS system), the concentration of BPA decreased significantly in 30 min with the increase of Fe(III) doping from 0.07% to 0.7%, which could be explained by the regeneration of Fe(III) to Fe(II) by reducing agents. It had been proved that transition metal Fe(II) could activate PMS to generate the reactive oxygen species (sulfate radicals ($SO_4^{\bullet-}$), hydroxyl radicals ($^{\bullet}OH$) and superoxide radical anions ($O_2^{\bullet-}$)) to degrade organic pollutants.

It should be noted that the degradation efficiency of BPA in the HAHC/MgAl-Fe(III)/PMS system was much higher than that in the Fe^{2+}/PMS system at such a low doping, and the latter was considered to be one of the most effective methods to activate PMS. The results showed that the addition of HAHC could effectively improve the degradation of BPA and the utilization of Fe atoms, thus avoiding the accumulation of Fe(III) in the HAHC/MgAl-Fe(III)/PMS system.

3.2.2. Effect of initial BPA concentration

The degradation efficiency of BPA decreased as the initial concentrations increased, which is shown in Fig. 5a.

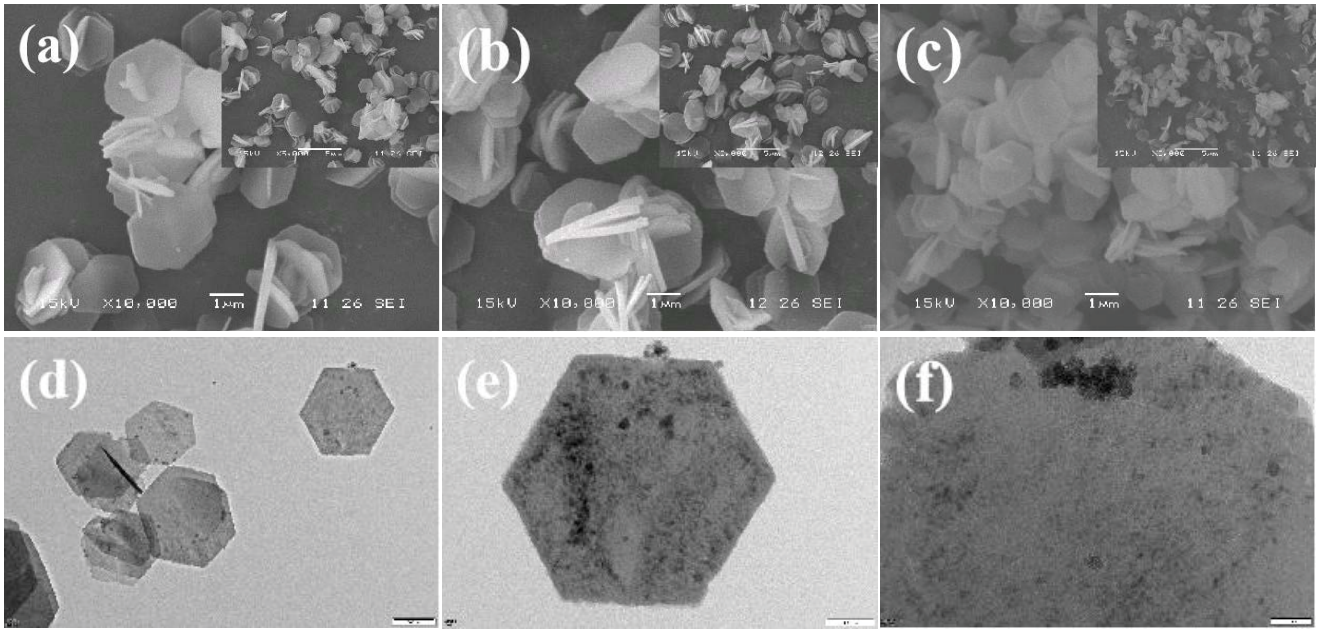

Fig. 2. SEM images of primary MgAlFe-LDH (a) 0.07%Fe-LDH, (b) 0.23%Fe-LDH, (c) 0.7%Fe-LDH and TEM images of primary 0.7%Fe-LDH (d–f).

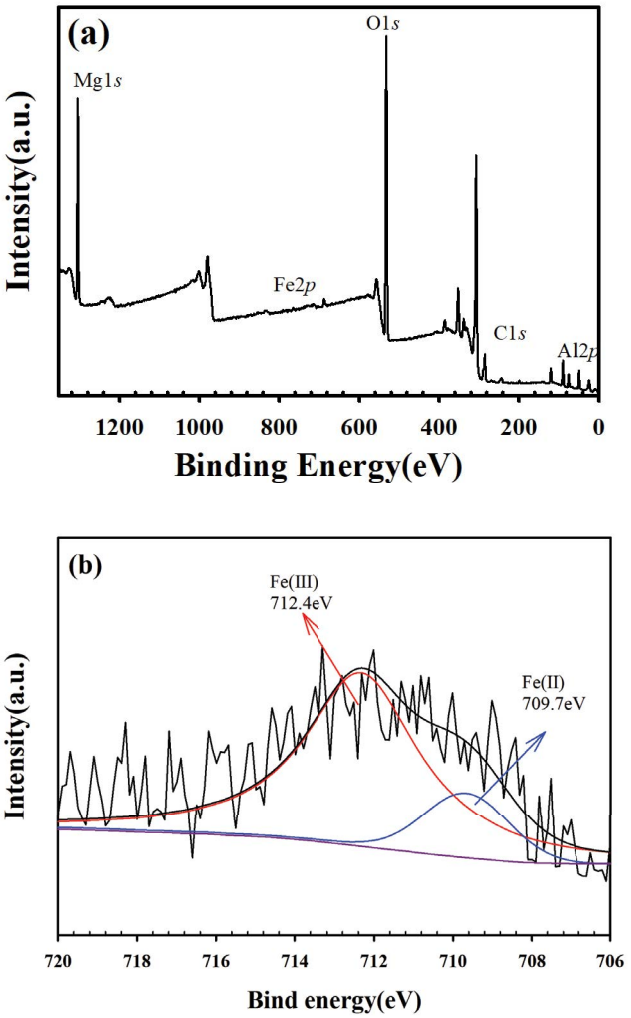

Fig. 3. XPS of primary 0.7%Fe-LDH (a) and Fe 2p in 0.7%Fe-LDH (b).

Considering that the degradation efficiency of BPA reached nearly 100% in 60 min when the concentration of BPA was 10 mg/L, the higher concentrations (20, 40 and 50 mg/L) were selected to evaluate the degradation effect of BPA in the HAHC/MgAl-Fe(III)/PMS system. When the initial BPA concentration increased from 10 to 50 mg/L, the degradation of BPA gradually decreased. Due to the limited generation of the reactive oxygen species, it was insufficient to completely degrade BPA at high concentration.

3.2.3. Effect of PMS concentration

The effect of PMS concentration on the degradation efficiency of BPA was also investigated. The PMS concentration was a key factor of the source of reactive oxygen species in the HAHC/MgAl-Fe(III)/PMS system, so the amount of PMS would influence the degradation of BPA by affecting the amount of reactive oxygen species. It can be seen from Fig. 5b that increasing the dosage of PMS from 0.1 to 1.5 g/L led to a considerable promotion of BPA degradation. When the initial concentration of PMS was 0.1 g/L, the removal rate

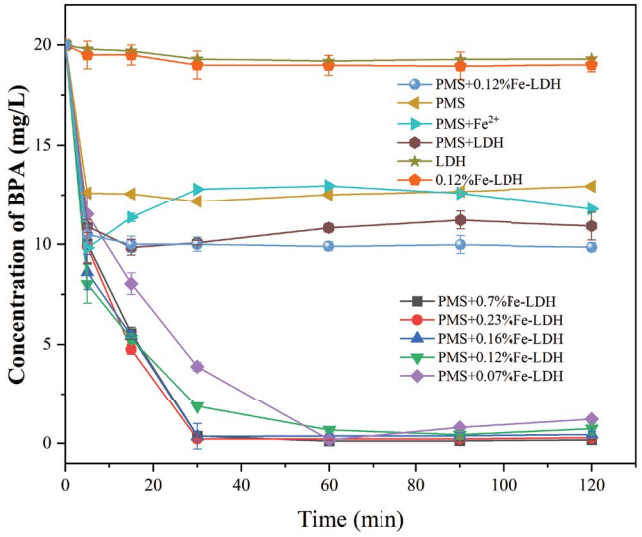

Fig. 4. Degradation of BPA in different PMS, LDH, MgAl-0.12%Fe(III), Fe^{2+}/PMS, MgAl/PMS, MgAl-0.12%Fe(III)/PMS, HAHC/MgAl-*x*%Fe(III)/PMS (*x* = 0.07, 0.12, 0.16, 0.23 and 0.7) processes. Conditions: $[MgAl]_0$ = 1.0 g/L, $[MgAl\text{-}x\%Fe(III)]_0$ = 1.0 g/L, $[PMS]_0$ = 1.0 g/L, $[Fe(II)]_0$ = 0.02 mM, $[HAHC]_0$ = 0.01 M, $[BPA]_0$ = 20 mg/L, pH_0 = 7.0, T = 25°C. Error bars represent the standard deviation from at least duplicate experiments.

of BPA was low and only 43.13% of BPA was removed over 120 min. Meanwhile, when PMS concentration increases from 0.5, 0.8, 1.0 to 1.5 g/L, the removal rate increases from 64.72%, 91.02%, 96.99% to 100%, respectively. It was worth noting that the removal rate increases more slowly with the increase of PMS concentration. This phenomenon may be attributed to the following aspects: (1) Because the dose of HAHC and MgAlFe-LDH was fixed, excessive PMS cannot generate more reactive oxygen species. (2) Adding excessive PMS may result in the potential quenching of sulfate radicals by residual PMS and sulfate radicals. (3) The competition by degradation intermediates of BPA may affect the degradation rate of BPA.

3.2.4. Effect of the dosage of MgAlFe-LDH

In order to explore the role of MgAlFe-LDH, the effect of 0.12%Fe-LDH concentration on BPA degradation in the HAHC/MgAl-Fe(III)/PMS process was studied. As shown in Fig. 5c, increased degradation of BPA was observed with the increase of MgAlFe-LDH concentration in the range of 0.5 to 1.0 g/L, then the increase in MgAlFe-LDH concentration resulted in a decrease in BPA removal. For example, the removal rate of BPA was 93.86% with MgAlFe-LDH dosage of 1.0 g/L in 120 min. In contrast, the removal rate of BPA decreased significantly with MgAlFe-LDH dosage of 3.0 g/L in the same period. As the dosage of MgAlFe-LDH increased, the sulfate radicals generated by PMS were sufficient to degrade more BPA in solution, while the amount of sulfate radicals was also determined by the concentration of PMS, which limited the degradation efficiency of BPA partly. Therefore, the dosage of MgAlFe-LDH controlled at 1.0 g/L was suitable in this experiment.

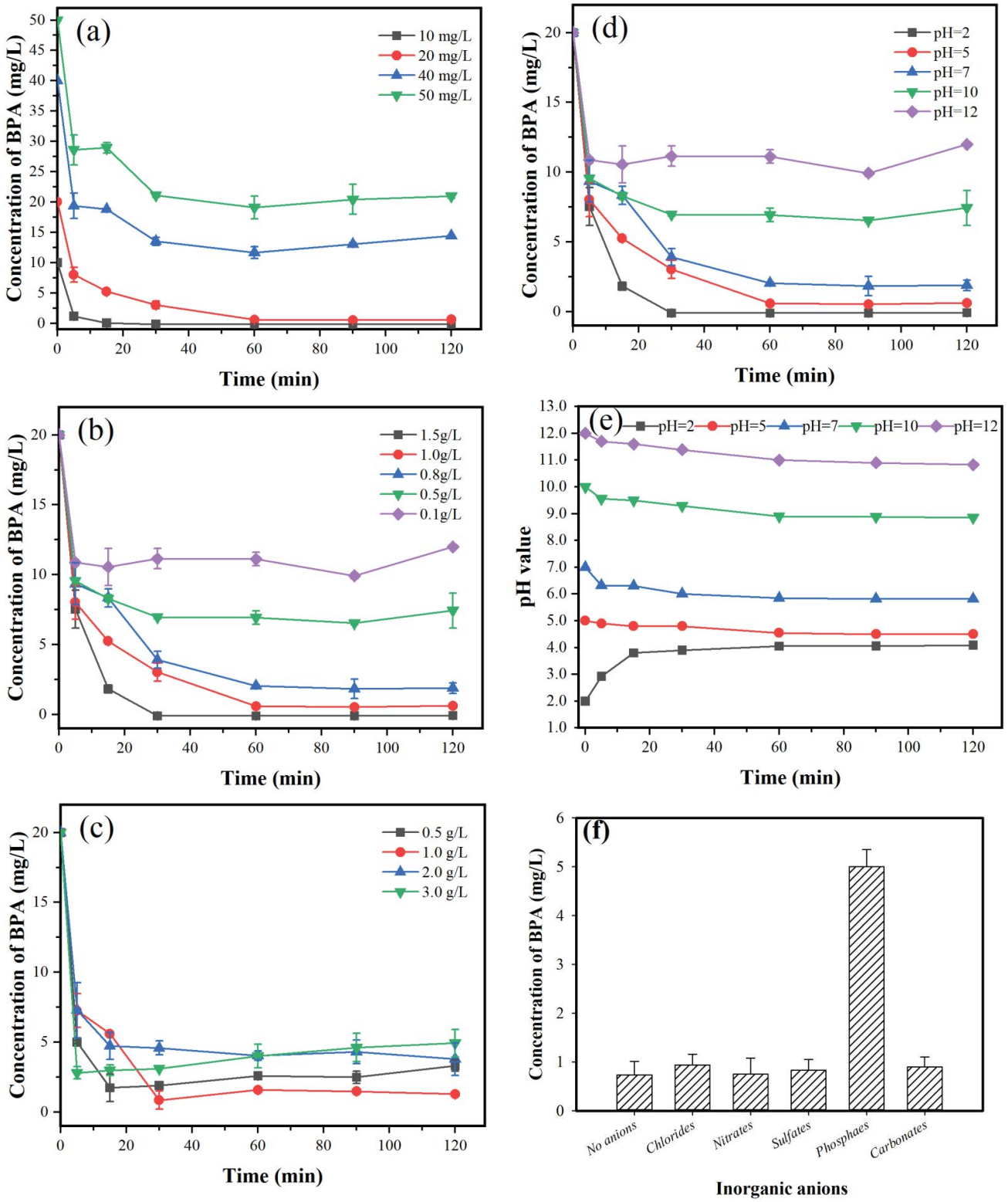

Fig. 5. Effect of (a) BPA concentration, (b) PMS concentration on, (c) MgAlFe-LDH concentration, (d) initial pH BPA degradation. (e) pH value change during reaction process. And (f) effect of inorganic anions on BPA degradation. Conditions: $[BPA]_0$ = 20 mg/L, $[PMS]_0$ = 1.0 g/L, $[0.12\%Fe\text{-}LDH]_0$ = 1.0 g/L, $[HAHC]_0$ = 0.01 M, [inorganic anion]$_0$ = 0.01 M, pH_0 = 7.0, T = 25°C.

3.2.5. Effect of initial pH

Effect of initial pH on BPA degradation was further evaluated in the HAHC/MgAl-Fe(III)/PMS system. As shown in Fig. 5d, the degradation of BPA insignificantly changed when the pH increased from 2.0 to 10.0, but was declined obviously when the pH further increased from 10.0 to 12.0. Hence, the neutral and acidic pH was most favorable for the degradation of BPA in the HAHC/MgAl-Fe(III)/PMS system, and the decomposition of one molar persulfate would yield two molar equiv. of protons. These results could be attributed to the fact that hydrogen ions could promote the conversion of peroxymonosulfate into sulfate radical under acidic conditions, which increases the concentration of sulfate radicals. Therefore, the degradation efficiency of BPA was higher under acidic conditions. Meanwhile, as reported in some literature, sulfate radical had a wider range of pH (3 ~ 10), which was different from the traditional Fenton oxidation technology that needed to keep the pH of the system at 2.8 ~ 3.5 [47]. Higher pH values led to the precipitation of Fe(III) into $Fe(OH)_3$, which consequently inhibited the regeneration of Fe(II) by HAHC [48,49] Apart from these, the change of solution pH values with reaction time during the BPA degradation process is recorded in Fig. 5e. While the initial pH was 2, 5 and 7, the pH was changed to 4.09, 4.50 and 5.81, respectively after 120 min reaction process. The buffer capacity of the HAHC/MgAl-Fe(III)/PMS system maintains the solution in acidic, and thus its efficiency for BPA removal remained high, which is consistent with the results of Qi et al. [50]. However, a further increase of pH exceeded the buffering capacity of the system and led to the formation of $Fe(OH)_3$, causing a significant decrease in degradation efficiency of BPA. Therefore, the HAHC/MgAl-Fe(III)/PMS system was highly efficient degradation efficiency in the degradation of organic matter, which was of great significance in real water treatment under acidic and neutral conditions.

3.2.6 Effect of inorganic ions

Natural aquatic bodies are usually a complex environment with the presence of a large number of anions, such as nitrate ions (NO_3^-), carbonate ions (CO_3^{2-}), chloride ions (Cl^-), sulfate ions (SO_4^{2-}) and phosphate ions (PO_4^{3-}). It is necessary to discuss the influence of these ions in BPA degradation system (Fig. 5f). As can be seen, the addition of Cl^-, NO_3^-, CO_3^{2-}, and SO_4^{2-} had negligible influence on the removal performance of HAHC/MgAl-Fe(III)/PMS system. Zhou et al. [51] had reported slight inhibition of Cl^- in AOPs process. It was attributed to the generation of less reactive species ($^{\bullet}Cl$, Cl_2 and HOCl) [Eqs. (1)–(3)], which had reported in Mn-doped $BiFeO_3$ nanoparticles/PMS system for BPA removal [52]. Similarly, carbonates can scavenges both $^{\bullet}OH$ and $SO_4^{\bullet-}$ radicals [Eqs. (4) and (5)] which was consistent with the research of Li et al. [53]. Furthermore, we can find that the generation of OH may increase the pH of solution, leading to PMS decomposition and iron ion precipitation. For nitrate ions, the BPA removal was completely consistent with that of no onions, indicating that the new radicals of $^{\bullet}NO_3^-$ can degrade the BPA [54]. In contrast, phosphate ions had a strong inhibitory effect on the degradation of BPA. This result may be due to the scavenging effect of phosphate on free radicals ($^{\bullet}OH$ and $SO_4^{\bullet-}$) [Eqs. (7)–(9)] [55]. Secondly, phosphate ions can chelate with surface Fe(III) to form inner-sphere complex, which occupy the active radical sites of LDH [56].

$$HSO_5^- + Cl^- \rightarrow SO_4^{2-} + HOCl \quad (1)$$

$$HSO_5^- + 2Cl^- + H^+ \rightarrow SO_4^{2-} + H_2O + Cl_2 \quad (2)$$

$$SO_4^{\bullet-} + Cl^- \rightarrow SO_4^- + Cl^{\bullet} \quad (3)$$

$$CO_3^{2-} + SO_4^{\bullet-} \rightarrow SO_4^{2-} + {}^{\bullet}CO_3^- \quad (4)$$

$$SO_4^{\bullet-} + {}^{\bullet}OH \rightarrow {}^{\bullet}CO_3^- + OH^- \quad (5)$$

$$SO_4^{\bullet-}/{}^{\bullet}OH + NO_3^- \rightarrow {}^{\bullet}NO_3^- + SO_4^-/OH^- \quad (6)$$

$$SO_4^{\bullet-} + HPO_4^{2-} \rightarrow SO_4^{2-} + HPO_4^{\bullet-} \quad (7)$$

$$SO_4^{\bullet-} + H_2PO_4^- \rightarrow SO_4^{2-} + H_2PO_4^{\bullet-} \quad (8)$$

$$^{\bullet}OH + H_2PO_4^- \rightarrow OH^- + H_2PO_4^{\bullet-} \quad (9)$$

3.2.7. Recycle of MgAlFe-LDH catalyst

As shown in Fig. 6, almost complete degradation of BPA was observed within 120 min of each run. This strongly indicates that MgAlFe-LDH can be recycled multiple times during the process and is a more environmentally-friendly

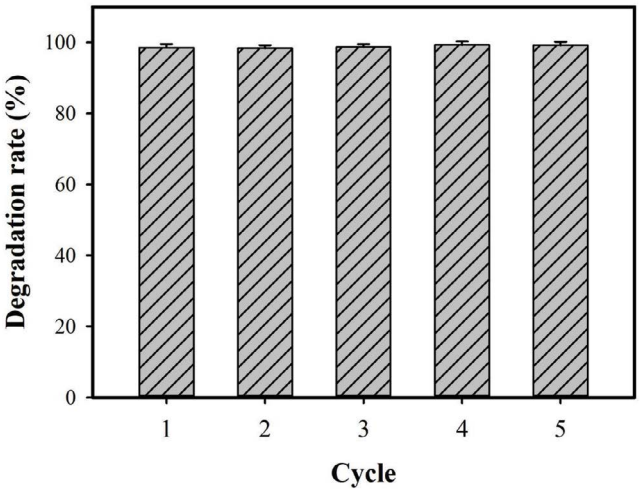

Fig. 6. Circulation experiment of MgAlFe-LDH degradation of BPA. Conditions: $[BPA]_0$ = 20 mg/L, $[PMS]_0$ = 1.0 g/L, $[0.12\%Fe\text{-}LDH]_0$ = 1.0 g/L, $[HAHC]_0$ = 0.01 M, T = 25°C.

material compared to other alternatives. As shown in characterization, the structure and morphology of catalyst did not collapse.

3.3. Scavenging tests for the reactive oxygen species identification in HAHC/MgAl-Fe(III)/PMS system

It has been reported that reactive oxygen species (ROS), such as hydroxyl radical, sulfate radical and superoxide radical, generated by activated persulfate, play an important role in BPA degradation. Owing to the high rate constants with $SO_4^{\bullet-}$ (k = 2.5 × 10^7 M/s and k = 8.2 × 10^7 M/s, respectively) and $^{\bullet}OH$ (k = 9.7 × 10^8 M/s and k = 1.9 × 10^9 M/s, respectively) [12], methanol (MeOH) and isopropanol (IPA) were effective quencher for both $SO_4^{\bullet-}$ and $^{\bullet}OH$ to investigate the effect on BPA degradation in Fig. 7a [57–60]. It was observed that the addition of whether MeOH (0.023 M) or IPA (0.016 M) affected on the degradation efficiency of BPA. As the concentration of BQ was 0.016 M, the degradation efficiency of BPA decreased to 32.28% in 120 min. The addition of BQ, which was used to quench $O_2^{\bullet-}$, demonstrated that $O_2^{\bullet-}$ was produced during the reaction and played an important role in the degradation of BPA. However, none of the reactions were completely inhibited, indicating the presence of other active species in the reaction.

To further determine the reactive radicals involved in the reaction, electron paramagnetic resonance (EPR) experiments were performed using DMPO as the radical trapping agent. As shown in Fig. 7b, the signal intensity ratios of DMPO-SO_4 and DMPO-OH were 1:1:1:1:1:1:1:1 and 1:2:2:1, respectively, suggesting that Fe(III) reduced by the addition of HAHC can activate PMS to generate sulfate radicals and hydroxyl radicals. Fig. 7c shows that the peaks characteristic of the DMPO-$O_2^{\bullet-}$ adduct appeared in the EPR spectrum of the MgAl-Fe(III), indicating that the $O_2^{\bullet-}$ radicals presented in the HAHC/MgAl-Fe(III)/PMS system [61]. This result was consistent that the BPA concentration did not decrease consistently the addition of *p*-benzoquinone in Fig. 7a. Meanwhile, the concentration of BPA continued to decrease from 15 to 30 min, which corresponded to the lack of weakening of sulfate radicals and hydroxyl radicals generated from 15 to 30 min shown in the EPR spectrum. These results suggest that $SO_4^{\bullet-}$, $^{\bullet}OH$ and $O_2^{\bullet-}$ played an essential role in the degradation of BPA.

3.4. Mechanism and pathways of BPA degradation in HAHC/MgAl-Fe(III)/PMS system

3.4.1. Characterization of post-reaction catalyst

However, in the obtained XRD spectra (Fig. 8a), there was no obvious structural change in the LDHs after the involvement of Fe(III) in the reaction. The reacted LDHs still showed clear diffraction peaks, as in the original LDH (Fig. 1a), indicating that the LDH reduced by HAHC still have high structural stability after reaction with PMS. As shown in Fig. 8b, the new absorption peak at 1,113 cm^{-1} of post-reaction MgAlFe-LDH could be attributed to the bending vibration of C–O–H, which may be the absorption of alcohols and phenols, indicating partial BPA was adsorbed on the material. The SEM of post-reaction MgAlFe-LDH still exhibited a hexagonal sheet-like morphology, exhibiting catalyst excellent stability and reusability (Fig. 9). Compared to the material before the reaction, the TEM image of post-reaction MgAlFe-LDH had become thinner, indicating Fe involvement the reaction (Fig. 9). As shown in Fig. 10, two

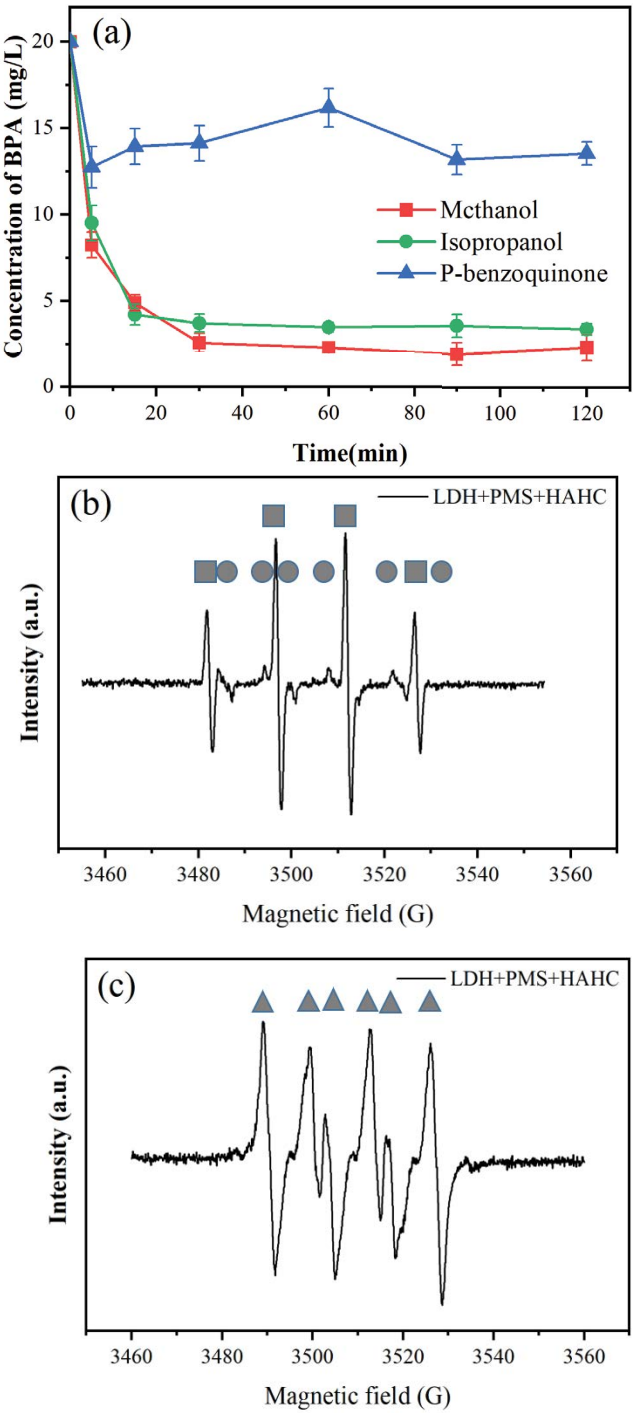

Fig. 7. (a) Effect of the inhibitors of BPA degradation, (b and c) EPR spectrum using DMPO. Conditions: $[BPA]_0$ = 20 mg/L, $[PMS]_0$ = 1.0 g/L, $[0.12\%Fe\text{-}LDH]_0$ = 1.0 g/L, $[HAHC]_0$ = 0.01 M, T = 25°C. Grey square: DMPO-OH, grey circle: DMPO-SO_4, grey triangle: DMPO-O_2^-.

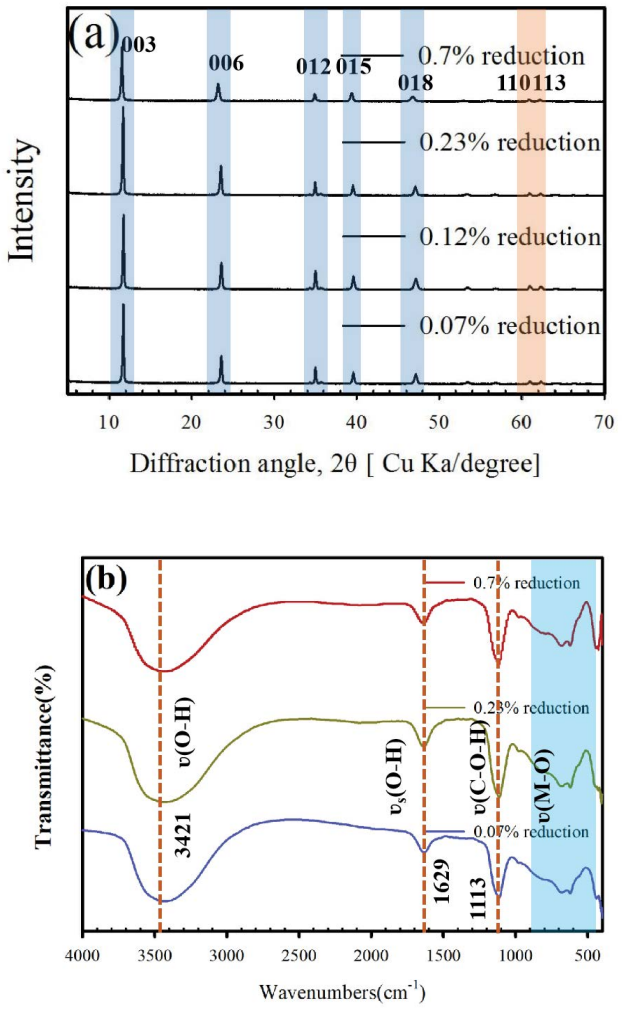

Fig. 8. (a) XRD spectra of post-reaction MgAlFe-LDH and (b) FTIR spectra of post-reaction MgAlFe-LDH.

different peaks centered at 712.1 and 710.2 eV were obtained by deconvolution of Fe $2p_{3/2}$, corresponding to Fe^{3+} and Fe^{2+} in the catalyst after the reaction. However, based on the Fe 2p envelop, the Fe^{2+}/Fe^{3+} value changed from 0.26 before the reaction to 0.54 after the reaction. This result implied the electron transfer between Fe^{2+} and Fe^{3+}, and thus the catalyst role of Fe in PMS activation.

In conclusion, the above results suggested that $\equiv Fe^{2+}$ and $\equiv Fe^{3+}$ were involved in the PMS oxidation reaction, with the $SO_4^{\bullet-}$, $^{\bullet}OH$ and $O_2^{\bullet-}$ radicals being the main reacting species, which further demonstrated the importance of HAHC in the cycling of Fe^{2+} and Fe^{3+}.

3.4.2. PMS activation mechanism and degradation pathway of BPA

It has been reported various reducing agents (RA) (including hydroxylamine (HA), sodium thiosulfate (STS), ascorbic acid (AA), sodium ascorbate (SA) and sodium sulfite (SS)) to accelerate the regeneration of Fe(II) in homogeneous system [35]. In this study, this experiment attempts to promote the degradation of BPA and improve the utilization of Fe atoms by adding HAHC to reduce Fe(III) [Eq. (10)]. Then, Fe(II)-activated PMS system could produce $SO_4^{\bullet-}$, while the reaction reactivity of Fe(III) with PMS was low [Eqs. (11) and (12)]. Furthermore, $SO_4^{\bullet-}/SO_5^{\bullet-}$ can react with H_2O/OH^- and produce hydroxyl radicals ($^{\bullet}OH$) and superoxide radical anions ($O_2^{\bullet-}$), which also facilitate the degradation of pollutants [Eqs. (12) ~ (17)] [62]. Therefore, both $^{\bullet}OH$, $SO_4^{\bullet-}$ and $O_2^{\bullet-}$ with high oxidation properties would attack BPA and cause its decomposition [63].

$$\equiv Fe^{3+} + 2NH_3OH^+ \rightarrow \equiv Fe^{2+} + \text{nitrogenous products} \quad (10)$$

$$\equiv Fe^{3+} + HSO_5^- \rightarrow \equiv Fe^{2+} + SO_5^{-\bullet} + H^+ \quad (11)$$

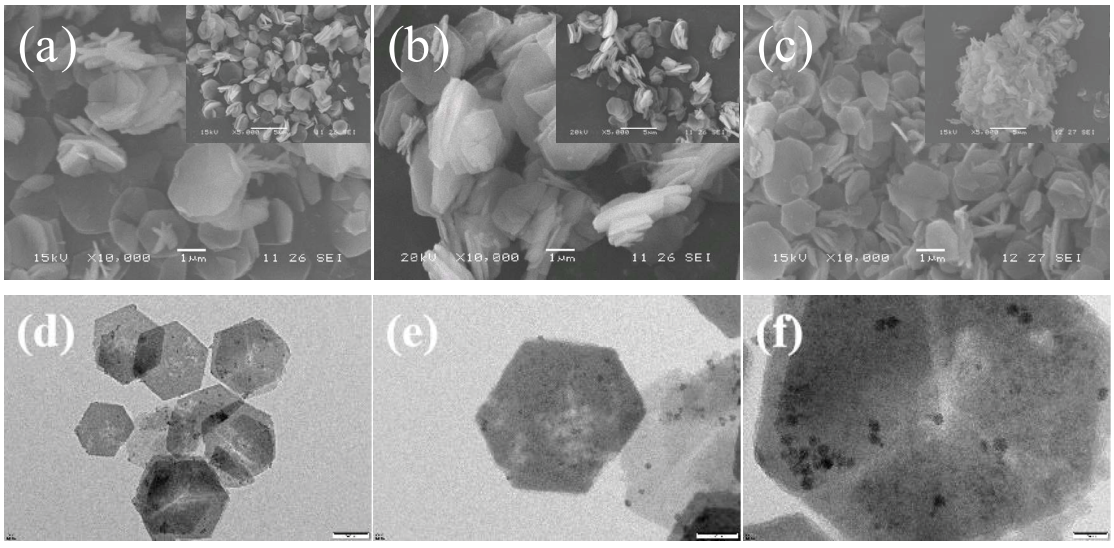

Fig. 9. SEM images of post-reaction MgAlFe-LDH (a) 0.07%Fe-LDH, (b) 0.23%Fe-LDH, (c) 0.7%Fe-LDH and TEM images of primary 0.7%Fe-LDH (d–f).

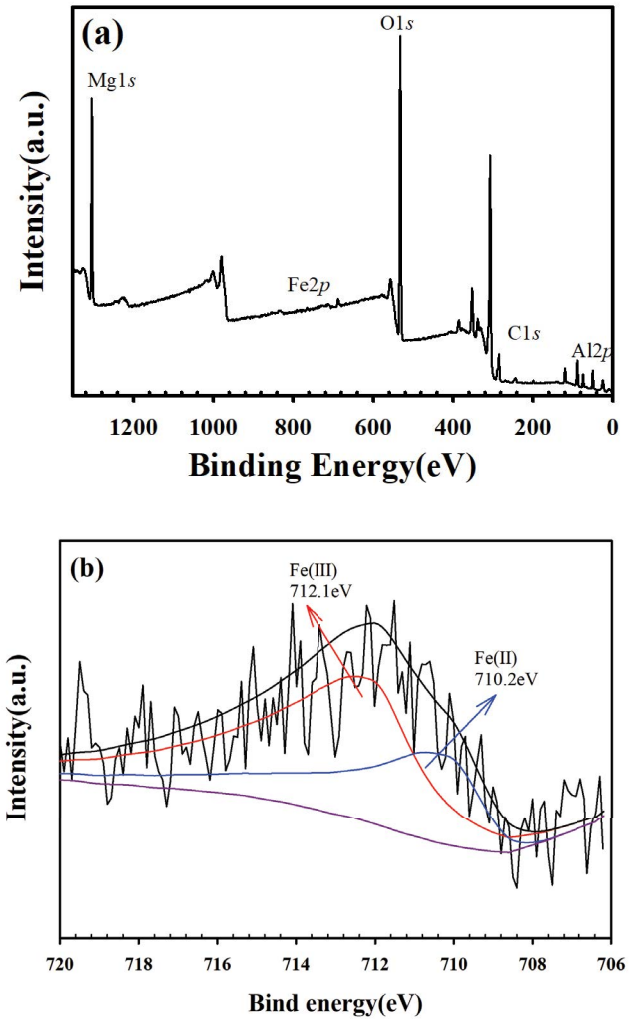

Fig. 10. XPS of post-reaction 0.7%Fe-LDH (a) and Fe 2p in 0.7%Fe-LDH (b).

$$\equiv Fe^{2+} + HSO_5^- \rightarrow \equiv Fe^{3+} + SO_4^{-\bullet} + OH^- \quad (12)$$

$$SO_5^{-\bullet} + 2OH_5^- \rightarrow 2SO_4^{2-} + 2HO^{\bullet} + O_2 \quad (13)$$

$$\left[{}_3^-O - S - O - O^-\right] + OH^- \rightarrow OH_2^- + SO_4^{2-} \quad (14)$$

$$SO_5^{2-} + HO_2^- \rightarrow SO_4^{2-} + O_2^{-\bullet} + H^+ \quad (15)$$

$$SO_4^{-\bullet} + OH^- \rightarrow SO_4^{2-} + HO^{\bullet} \quad (16)$$

$$SO_4^{-\bullet} + H_2O \rightarrow SO_4^{2-} + HO^{\bullet} + H^+ \quad (17)$$

In order to obtain the degradation pathway of BPA in the HAHC system, the HPLC-MS was used to analysis the generation of intermediates after 120 min. Combined with the previous literature, possible severa intermediates was identified as benzophenone, benzaldehyde, p-hydroxybenzoic acid, 4-(prop-1-en-2yl)benzene-1,2-diol,4-hydroxyacetophenone, 2,5-cyclohexadienol, etc. In the present study, firstly, $^{\bullet}OH$, $SO_4^{\bullet-}$ and $O_2^{\bullet-}$ generated from [Eqs. (12)~(17)] directly attacked the isopropyl group in BPA to be oxidized as alcohol and carboxyl groups and formed 1-hydroxy-2,2-bis(4-hydroxyphenyl) propionic acid (MW = 274) [64]. The result was consistent with the intermediates produced by the degradation of BPA using vanadium-titanium magnetite activated PMS by Lai et al. [30]. Subsequently, biphenyl-type compound compounds were generated due to the continued attack of hydroxyl radicals and finally cleavage to produce benzoquinone and 2,5-cyclopentadienol. The para-carbon atom of BPA was susceptible to attack by free radicals, causing the β-bond of BPA to break, forming p-isopropenyl (IPP) phenol and phenol, which were further oxidized

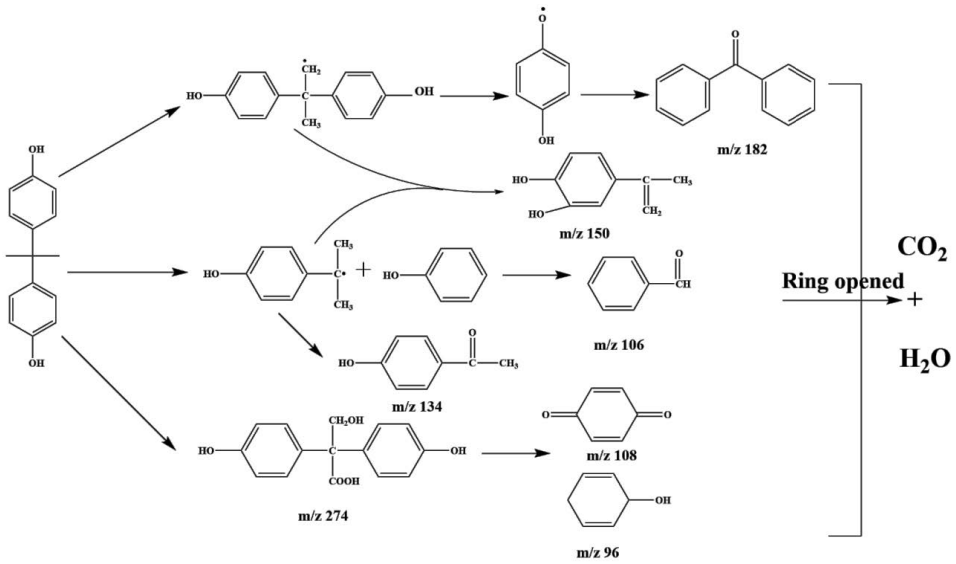

Fig. 11. Possible pathways for the degradation of BPA.

to benzaldehyde. Isopropyl phenol (IPP) could be generated by deprotonation of the isopropyl phenol cation, while IPP may generate 4-(prop-1-en-2yl)benzene-1,2-diol, p-hydroxybenzoic acid. Besides the addition reaction on the aromatic ring, HO• generated from SO_3^{2-} [Eq. (13)] also could attack the C atom on the sp^3 heteromethyl group of the BPA molecule and a C–C break occurs to produce para-phenoxy and p-isopropenyl phenol (IPP) [65]. Oxidation of para-phenoxy produces benzophenone which is further oxidized to produce benzaldehyde. Finally, due to the strong oxidizing power of free radicals, the above intermediates further react to form ring-opening products, which are then mineralized to CO_2 and H_2O (Fig. 11).

4. Conclusion

In this study, the degradation of BPA was observed to be over 90% within 120 min by adding a reducing agent (HAHC) into LDH/PMS system. With the low Fe doping, the addition of HAHC effectively promoted the utilization of iron atoms and the transformation of Fe(III), avoiding the accumulation of Fe(III) to improve the degradation efficiency of BPA. Meanwhile, the catalyst could be applied in a wide pH range (2~10) and recycled several times to degrade BPA. In addition, the radical scavenging experiment certified the main reactive oxygen species were sulfate radical ($SO_4^{\bullet-}$), hydroxyl radical (•OH) and superoxide radical ($O_2^{\bullet-}$) in the HAHC /LDH/PMS process. In conclusion, activation of PMS by adding reducing agents to promote Fe(III)-LDH is a promising water treatment technology, but its widespread practical application requires careful consideration of the complex groundwater composition.

Acknowledgement

This study was funded by the National Natural Science Foundation of China (No. 2018YFC1802701), National Natural Science Foundation of China (41703119 and 51504170), and Graduate Education Innovation Foundation of Wuhan Institute of Technology.

References

[1] Y. Deng, R. Zhao, Advanced oxidation processes (AOPs) in wastewater treatment, Curr. Pollut. Rep., 1 (2015) 167–176.
[2] K.H. Chan, W. Chu, Degradation of atrazine by cobalt-mediated activation of peroxymonosulfate: different cobalt counteranions in homogenous process and cobalt oxide catalysts in photolytic heterogeneous process, Water Res., 43 (2009) 2513–2521.
[3] L. Hu, G. Zhang, M. Liu, Q. Wang, P. Wang, Optimization of the catalytic activity of a $ZnCo_2O_4$ catalyst in peroxymonosulfate activation for bisphenol A removal using response surface methodology, Chemosphere, 212 (2018) 152–161.
[4] W.D. Oh, Z. Dong, T.T. Lim, Generation of sulfate radical through heterogeneous catalysis for organic contaminants removal: current development, challenges and prospects, Appl. Catal., B, 194 (2016) 169–201.
[5] Y.F. Huang, Y.H. Huang, Identification of produced powerful radicals involved in the mineralization of bisphenol A using a novel UV-$Na_{(2)}S_{(2)}O_{(8)}$/$H_{(2)}O_{(2)}$-Fe(II,III) two-stage oxidation process, J. Hazard. Mater., 162 (2009) 1211–1216.
[6] S.B. Hammouda, F. Zhao, Z. Safaei, D.L. Ramasamy, B. Doshi, M. Sillanpää, Sulfate radical-mediated degradation and mineralization of bisphenol F in neutral medium by the novel magnetic Sr_2CoFeO_6 double perovskite oxide catalyzed peroxymonosulfate: influence of co-existing chemicals and UV irradiation, Appl. Catal., B, 233 (2018) 99–111.
[7] W. Wang, M. Chen, D. Wang, M. Yan, Z. Liu, Different activation methods in sulfate radical-based oxidation for organic pollutants degradation: catalytic mechanism and toxicity assessment of degradation intermediates, Sci. Total Environ., 772 (2021) 145522, doi: 10.1016/j.scitotenv.2021.145522.
[8] J. Peng, Z. Wang, S. Wang, J. Liu, Y. Zhang, B. Wang, Z. Gong, M. Wang, H. Dong, J. Shi, H. Liu, G. Yan, G. Liu, S. Gao, Z. Cao, Enhanced removal of methylparaben mediated by cobalt/carbon nanotubes (Co/CNTs) activated peroxymonosulfate in chloride-containing water: reaction kinetics, mechanisms and pathways, Chem. Eng. J., 409 (2021) 128176, doi: 10.1016/j.cej.2020.128176.
[9] Y. Qi, R. Qu, J. Liu, J. Chen, G. Al-Basher, N. Alsultan, Z. Wang, Z. Huo, Oxidation of flumequine in aqueous solution by UV-activated peroxymonosulfate: kinetics, water matrix effects, degradation products and reaction pathways, Chemosphere, 237 (2019) 124484, doi: 10.1016/j.chemosphere.2019.124484.
[10] P. Neta, R.E. Huie, A.B. Ross, Rate constants for reactions of inorganic radicals in aqueous solution, J. Phys. Chem. Ref. Data, 17 (1988) 1027–1284.
[11] A. Rastogi, S.R. Al-Abed, D.D. Dionysiou, Sulfate radical-based ferrous–peroxymonosulfate oxidative system for PCBs degradation in aqueous and sediment systems, Appl. Catal., B, 85 (2009) 171–179.
[12] Y.R. Wang, W. Chu, Degradation of 2,4,5-trichlorophenoxyacetic acid by a novel electro-Fe(II)/oxone process using iron sheet as the sacrificial anode, Water Res., 45 (2011) 3883–3889.
[13] J. Wang, S. Wang, Activation of persulfate (PS) and peroxymonosulfate (PMS) and application for the degradation of emerging contaminants, Chem. Eng. J., 334 (2017) 1502–1517.
[14] A. Latif, S. Kai, Y. Si, Catalytic degradation of organic pollutants in Fe(III)/peroxymonosulfate (PMS) system: performance, influencing factors, and pathway, Environ. Sci. Pollut. Res., 26 (2019) 36410–36422.
[15] L. Sbardella, I. Velo Gala, J. Comas, S. Morera Carbonell, I. Rodríguez-Roda, W. Gernjak, Integrated assessment of sulfate-based AOPs for pharmaceutical active compound removal from wastewater, J. Cleaner Prod., 260 (2020) 121014, doi: 10.1016/j.jclepro.2020.121014.
[16] C.S. Liu, K. Shih, C.X. Sun, F. Wang, Oxidative degradation of propachlor by ferrous and copper ion activated persulfate, Sci. Total Environ., 416 (2012) 507–512.
[17] M. Xu, X. Gu, S. Lu, Z. Qiu, Q. Sui, Z. Miao, X. Zang, X. Wu, Degradation of carbon tetrachloride in aqueous solution in the thermally activated persulfate system, J. Hazard. Mater., 286 (2015) 7–14.
[18] J. Rodríguez-Chueca, C. Amor, T. Silva, D. Dionysiou, J.A. Peres, Treatment of winery wastewater by sulphate radicals: HSO_5^-/transition metal/UV-A LEDs, Chem. Eng. J., 310 (2017) 473–483.
[19] C.M. Liu, Z.H. Diao, W.Y. Huo, L.J. Kong, J.J. Du, Simultaneous removal of Cu^{2+} and bisphenol A by a novel biochar-supported zero valent iron from aqueous solution: synthesis, reactivity and mechanism, Environ. Pollut., 239 (2018) 698–705.
[20] L. Chen, T. Luo, S. Yang, J. Xu, Z. Liu, F. Wu, Efficient metoprolol degradation by heterogeneous copper ferrite/sulfite reaction, Environ. Chem. Lett., 16 (2018) 599–603.
[21] J. Wang, B. Hasaer, M. Yang, R. Liu, C. Hu, H. Liu, J. Qu, Anaerobically-digested sludge disintegration by transition metal ions-activated peroxymonosulfate (PMS): comparison between Co^{2+}, Cu^{2+}, Fe^{2+} and Mn^{2+}, Sci. Total Environ., 713 (2020) 136530, doi: 10.1016/j.scitotenv.2020.136530.
[22] C. Tan, Y. Dong, L. Shi, Q. Chen, S. Yang, X. Liu, J. Ling, X. He, D. Fu, Degradation of Orange II in ferrous activated peroxymonosulfate system: efficiency, situ EPR spin trapping and degradation pathway study, J. Taiwan Inst. Chem. Eng., 83 (2018) 74–81.
[23] L. Ling, D. Zhang, C. Fan, C. Shang, A Fe(II)/citrate/UV/PMS process for carbamazepine degradation at a very low Fe(II)/PMS ratio and neutral pH: the mechanisms, Water Res., 124 (2017) 446–453.

[24] W. Peng, Y. Dong, Y. Fu, L. Wang, Z. Wang, Non-radical reactions in persulfate-based homogeneous degradation processes: a review, Chem. Eng. J., 421 (2021) 127818, doi: 10.1016/j.cej.2020.127818.
[25] J. Yan, L. Min, L. Zhu, M.N. Anjum, Z. Jing, H. Tang, Degradation of sulfamonomethoxine with Fe_3O_4 magnetic nanoparticles as heterogeneous activator of persulfate, J. Hazard. Mater., 186 (2011) 1398–1404.
[26] Y. Zhou, X. Wang, C. Zhu, D.D. Dionysiou, G. Zhao, G. Fang, D. Zhou, New insight into the mechanism of peroxymonosulfate activation by sulfur-containing minerals: role of sulfur conversion in sulfate radical generation, Water Res., 142 (2018) 208–216.
[27] P. Hu, M. Long, Cobalt-catalyzed sulfate radical-based advanced oxidation: a review on heterogeneous catalysts and applications, Appl. Catal., B, 181 (2016) 103–117.
[28] S. Xiao, M. Cheng, H. Zhong, Z. Liu, Y. Liu, X. Yang, Q. Liang, Iron-mediated activation of persulfate and peroxymonosulfate in both homogeneous and heterogeneous ways: a review, Chem. Eng. J., 384 (2020) 123265, doi: 10.1016/j.cej.2019.123265.
[29] Y. Feng, D. Wu, H. Li, J. Bai, Y. Hu, C. Liao, X.-y. Li, K. Shih, Activation of persulfates using siderite as a source of ferrous ions: sulfate radical production, stoichiometric efficiency, and implications, ACS Sustainable Chem. Eng., 6 (2018) 3624–3631.
[30] L. Lai, H. Zhou, B. Lai, Heterogeneous degradation of bisphenol A by peroxymonosulfate activated with vanadium-titanium magnetite: performance, transformation pathways and mechanism, Chem. Eng. J., 349 (2018) 633–645.
[31] M. Jin, M. Long, H. Su, P. Yue, Y. Zhang, Magnetically separable maghemite/montmorillonite composite as an efficient heterogeneous Fenton-like catalyst for phenol degradation, Environ. Sci. Pollut. Res., 24 (2016) 1926–1937.
[32] L.H. Hou, X.M. Li, Q. Yang, F. Chen, S.N. Wang, Y.H. Ma, Y. Wu, X.F. Zhu, X.D. Huang, D.B. Wang, Heterogeneous activation of peroxymonosulfate using Mn-Fe layered double hydroxide: performance and mechanism for organic pollutant degradation, Sci. Total Environ., 663 (2019) 453–464.
[33] Y. Liu, J. Lang, T. Wang, A. Jawad, H. Wang, A. Khan, Z. Chen, Z. Chen, Enhanced degradation of isoproturon in soil through persulfate activation by Fe-based layered double hydroxide: different reactive species comparing with activation by homogenous Fe(II), Environ. Sci. Pollut. Res., 25 (2018) 26394–26404.
[34] X. Wu, X. Gu, S. Lu, M. Xu, X. Zang, Z. Miao, Z. Qiu, S. Qian, Degradation of trichloroethylene in aqueous solution by persulfate activated with citric acid chelated ferrous ion, Chem. Eng. J., 255 (2014) 585–592.
[35] X. Wu, X. Gu, S. Lu, Z. Qiu, Q. Sui, X. Zang, Z. Miao, M. Xu, Strong enhancement of trichloroethylene degradation in ferrous ion activated persulfate system by promoting ferric and ferrous ion cycles with hydroxylamine, Sep. Purif. Technol., 147 (2015) 186–193.
[36] J. Zou, J. Ma, L. Chen, X. Li, Y. Guan, P. Xie, C. Pan, Rapid acceleration of ferrous iron/peroxymonosulfate oxidation of organic pollutants by promoting Fe(III)/Fe(II) cycle with hydroxylamine, Environ. Sci. Technol., 47 (2013) 11685–11691.
[37] H. Tamura, K. Goto, T. Yotsuyanagi, M. Nagayama, Spectrophotometric determination of iron(II) with 1,10-phenanthroline in the presence of large amounts of iron(III), Talanta, 21 (1974) 314–318.
[38] Z. Miao, X. Gu, S. Lu, M.L. Brusseau, N. Yan, Z. Qiu, Q. Sui, Enhancement effects of reducing agents on the degradation of tetrachloroethene in the Fe(II)/Fe(III) catalyzed percarbonate system, J. Hazard. Mater., 300 (2015) 530–537.
[39] X. Xue, Q. Gu, G. Pan, J. Liang, G. Huang, G. Sun, S. Ma, X. Yang, Nanocage structure derived from sulfonated beta-cyclodextrin intercalated layered double hydroxides and selective adsorption for phenol compounds, Inorg. Chem., 53 (2014) 1521–1529.
[40] J.W. Zhao, L.D. Deng, W. Zheng, S. Xu, Q.Q. Yu, X.H. Qiu, Nickel-induced structure transformation in hydrocalumite for enhanced ammonia decomposition, Int. J. Hydrogen Energy, 45 (2020) 12244–12255.
[41] P. Zhong, Q. Yu, J. Zhao, S. Xu, X. Qiu, J. Chen, Degradation of bisphenol A by Fe-Al layered double hydroxides: a new synergy of homo- and heterogeneous Fenton systems, J. Colloid Interface Sci., 552 (2019) 122–133.
[42] S. Xu, J. Zhao, L. Deng, J. Niu, X. Zhou, S. Zhang, X. Qiu, J. Chen, Adsorption mechanism of borate with different calcined layered double hydroxides in a molar ratio of 3:1, Desal. Water Treat., 155 (2019) 296–310.
[43] X. Zhong, Z. Zhang, T. Zhou, P. Lu, J. Cheng, S. Chen, Z. Shu, Y. Hong, Q. Wang, A. Umar, Flower-shaped $Mg_3Al_{1-x}Fe_x$-CO_3 layered double hydroxides derived adsorbents with tunable memory effect for environmental remediation, J. Nanosci. Nanotechnol., 18 (2018) 2609–2615.
[44] Z. Gao, K. Sasaki, X. Qiu, Structural memory effect of Mg-Al and Zn-Al layered double hydroxides in the presence of different natural humic acids: process and mechanism, Langmuir, 34 (2018) 5386–5395.
[45] M. Hadnadjev, T. Vulic, R. Marinkovic-Neducin, Y. Suchorski, H. Weiss, The iron oxidation state in Mg–Al–Fe mixed oxides derived from layered double hydroxides: an XPS study, Appl. Surf. Sci., 254 (2018) 4297–4302.
[46] C. Liang, C.J. Bruell, M.C. Marley, K.L. Sperry, Persulfate oxidation for in situ remediation of TCE. II. Activated by chelated ferrous ion, Chemosphere, 55 (2004) 1225–1233.
[47] C. Liang, C.P. Liang, C.C. Chen, pH dependence of persulfate activation by EDTA/Fe(III) for degradation of trichloroethylene, J. Contam. Hydrol., 106 (2009) 173–182.
[48] L. Zhou, J. Hu, H. Zhong, X. Li, Study of phenol removal using fluidized-bed Fenton process, Chem. Eng. Res. Des., 90 (2012) 377–382.
[49] Z. Liao, S. Dai, S. Long, Y. Yu, J. Ali, H. Wang, Z. Chen, Z. Chen, Pd based in situ AOPs with heterogeneous catalyst of FeMgAl layered double hydrotalcite for the degradation of bisphenol A and landfill leachate through multiple pathways, Environ. Sci. Pollut. Res., 25 (2018) 35623–35636.
[50] S.K. Rani, D. Easwaramoorthy, I.M. Bilal, M. Palanichamy, Studies on Mn(II)-catalyzed oxidation of α-amino acids by peroxomonosulphate in alkaline medium-deamination and decarboxylation: a kinetic approach, Appl. Catal., A, 369 (2009) 1–7.
[51] J. Zhou, J. Xiao, D. Xiao, Y. Guo, C. Fang, X. Lou, J. Liu, Transformations of chloro and nitro groups during the peroxymonosulfate-based oxidation of 4-chloro-2-nitrophenol, Chemosphere, 134 (2015) 446–451.
[52] S.B. Hammouda, F. Zhao, Z. Safaei, D.L. Ramasamy, B. Doshi, M. Sillanpää, Sulfate radical-mediated degradation and mineralization of bisphenol F in neutral medium by the novel magnetic Sr_2CoFeO_6 double perovskite oxide catalyzed peroxymonosulfate: influence of co-existing chemicals and UV irradiation, Appl. Catal., B, 233 (2018) 99–111.
[53] B. Li, J. Zhu, Simultaneous degradation of 1,1,1-trichloroethane and solvent stabilizer 1,4-dioxane by a sono-activated persulfate process, Chem. Eng. J., 284 (2016) 750–763.
[54] T. Soltani, A. Tayyebi, B.K. Lee, Quick and enhanced degradation of bisphenol A by activation of potassium peroxymonosulfate to SO_4 center dot-with Mn-doped $BiFeO_3$ nanoparticles as a heterogeneous Fenton-like catalyst, Appl. Surf. Sci., 441 (2018) 853–861.
[55] W.D. Oh, Z. Dong, T.T. Lim, Generation of sulfate radical through heterogeneous catalysis for organic contaminants removal: current development, challenges and prospects, Appl. Catal., B, 194 (2016) 169–201.
[56] F. Qi, W. Chu, B. Xu, Modeling the heterogeneous peroxymonosulfate/Co-MCM41 process for the degradation of caffeine and the study of influence of cobalt sources, Chem. Eng. J., 235 (2014) 10–18.
[57] J.M. Monteagudo, A. Duran, I. San Martin, A. Carnicer, Roles of different intermediate active species in the mineralization reactions of phenolic pollutants under a UV-A/C photo-Fenton process, Appl. Catal., B, 106 (2011) 242–249.

[58] Y. Xu, J. Ai, H. Zhang, The mechanism of degradation of bisphenol A using the magnetically separable $CuFe_2O_4$/peroxymonosulfate heterogeneous oxidation process, J. Hazard. Mater., 309 (2016) 87–96.
[59] W. Nie, Q. Mao, Y. Ding, Y. Hu, H. Tang, Highly efficient catalysis of chalcopyrite with surface bonded ferrous species for activation of peroxymonosulfate toward degradation of bisphenol A: a mechanism study, J. Hazard. Mater., 364 (2019) 59–68.
[60] G.V. Buxton, C.L. Greenstock, W.P. Helman, A.B. Ross, Critical review of rate constants for reactions of hydrated electrons, hydrogen atoms and hydroxyl radicals ($^{\bullet}OH/^{\bullet}O^{-}$) in aqueous solution, J. Phys. Chem. Ref. Data, 17 (1988) 566–571.
[61] Y. Li, D. Li, S. Fan, T. Yang, Q. Zhou, Facile template synthesis of dumbbell-like Mn_2O_3 with oxygen vacancies for efficient degradation of organic pollutants by activating peroxymonosulfate, Catal. Sci. Technol., 10 (2020) 864–875.
[62] D. He, Y. Cheng, Y. Zeng, H. Luo, K. Luo, J. Li, X. Pan, D. Barcelo, J.C. Crittenden, Synergistic activation of peroxymonosulfate and persulfate by ferrous ion and molybdenum disulfide for pollutant degradation: theoretical and experimental studies, Chemosphere, 240 (2020) 124979, doi: 10.1016/j.chemosphere.2019.124979.
[63] X. Xu, D. Liu, W. Chen, S. Zong, Y. Liu, Waste control by waste: efficient removal of bisphenol A with steel slag, a novel activator of peroxydisulfate, Environ. Chem. Lett., 16 (2018) 1435–1440.
[64] X. Li, Z. Wang, B. Zhang, A.I. Rykov, M.A. Ahmed, J. Wang, $Fe_xCo_{3-x}O_4$ nanocages derived from nanoscale metal-organic frameworks for removal of bisphenol A by activation of peroxymonosulfate, Appl. Catal., B, 181 (2016) 788–799.
[65] L. Zhao, Y. Ji, D. Kong, J. Lu, Q. Zhou, X. Yin, Simultaneous removal of bisphenol A and phosphate in zero-valent iron activated persulfate oxidation process, Chem. Eng. J., 303 (2016) 458–466.